


Article

One-Pot Synthesis of Nano CuO-ZnO Modified Hydrochar Derived from Chitosan and Starch for the H₂S Conversion

Lihua Zang ^{1,2}, Chengxuan Zhou ², Liming Dong ¹, Leilei Wang ³, Jiaming Mao ⁴, Xiaomin Lu ⁵, Rong Xue ² and Yunqian Ma ^{1,2,*} 

¹ Key Laboratory of Cleaner Production and Integrated Resource Utilization of China National Light Industry, Beijing Technology and Business University, Beijing 100048, China; zlh@qlu.edu.cn (L.Z.); donglm@btbu.edu.cn (L.D.)

² College of Environmental Science and Engineering, Qilu University of Technology (Shandong Academy of Science), Jinan 250353, China; zhouchengxuan@ipe.ac.cn (C.Z.); xr@qlu.edu.cn (R.X.)

³ Ecology Institute of Shandong Academy of Sciences, Qilu University of Technology (Shandong Academy of Sciences), Jinan 250014, China; wangll@qlu.edu.cn

⁴ College of Environmental Science and Engineering, Beijing Forestry University, Beijing 100083, China; mjm2020@bjfu.edu.cn

⁵ Department of Forest Biomaterials, North Carolina State University, Raleigh, NC 27695, USA; xlu13@ncsu.edu

* Correspondence: mayq@qlu.edu.cn

Abstract: A novel kind of hydrochar adsorbent, modified by CuO-ZnO and derived from chitosan or starch, was synthesized for H₂S adsorption. The prepared adsorbent was characterized by BET, XRD, EDX, SEM, and XPS. The results showed that the modified hydrochar contained many amino groups as functional groups, and the nanometer metal oxide particles had good dispersion on the surface of the hydrochar. The maximum sulfur capacity reached 28.06 mg/g-adsorbent under the optimized conditions. The amine group significantly reduced the activation energy between H₂S and CuO-ZnO conducive to the rapid diffusion of H₂S among the lattices. Simultaneously, cationic polyacrylamide as a steric stabilizer could change the formation process of CuO and ZnO nanoparticles, which made the particle size smaller, enabling them to react with H₂S sufficiently easily. This modified hydrochar derived from both chitosan and starch could be a promising adsorbent for H₂S removal.

Keywords: hydrochar; adsorbent; mixed metal oxides; H₂S conversion



Citation: Zang, L.; Zhou, C.; Dong, L.; Wang, L.; Mao, J.; Lu, X.; Xue, R.; Ma, Y. One-Pot Synthesis of Nano CuO-ZnO Modified Hydrochar Derived from Chitosan and Starch for the H₂S Conversion. *Catalysts* **2021**, *11*, 767. <https://doi.org/10.3390/catal11070767>

Academic Editor: Daniela Barba

Received: 18 May 2021

Accepted: 15 June 2021

Published: 24 June 2021

Publisher's Note: MDPI stays neutral with regard to jurisdictional claims in published maps and institutional affiliations.



Copyright: © 2021 by the authors. Licensee MDPI, Basel, Switzerland. This article is an open access article distributed under the terms and conditions of the Creative Commons Attribution (CC BY) license (<https://creativecommons.org/licenses/by/4.0/>).

1. Introduction

Hydrogen sulfide (H₂S), a poisonous, odorous, and corrosive gas, commonly exists in industrial gases such as coal gasification gas, natural gas, and biogas. H₂S is harmful to humans and livestock, and it not only brings corrosion to metal pipes and reaction devices in the industrial production process, but also causes catalyst poisoning, which affects product quality [1,2]. H₂S is easy to burn, generating SO₂ as a combustion product. Whether through combustion or direct emissions, it can exert a severe impact on the atmospheric environment. Therefore, H₂S should be fixed on some materials or removed from the production process and environment.

At present, there are many industrial methods to remove H₂S. According to production conditions and desulfurization costs, the methods of H₂S removal in industrial processes can be classified into wet flue gas desulfurization (WFGD) and dry flue gas desulfurization (DFGD) [3,4]. The desulfurizer of WFGD is a liquid that absorbs and separates H₂S with large processing capacity and mature technology. WFGD has some disadvantages—for example, high energy consumption, secondary pollution, and high regeneration cost. DFGD has mainly been used to remove H₂S at low concentrations, and it has the advantages of high H₂S removal efficiency and low cost [5]. The commonly used

dry desulfurization methods in industrial processes are the zinc oxide method, iron oxide method, manganese desulfurization method, Claus method, etc. [6–10].

Biochar is defined as a solid, carbon-rich product obtained from biomass through various thermochemical technologies [11–14]. Pyrochar and hydrochar are two kinds of biochar prepared from the pyrolysis and hydrothermal carbonization (HTC) of biomass [15], respectively. The biomass includes straw, sawdust, the dung of herbivores, etc. [16]. Biochar is a promising alternative adsorbent for toxic gas and wastewater treatment [17,18]. Most researchers have focused on pyrochar, but there are a few reports on the application of hydrochar in H₂S capture. HTC is an auspicious approach for the use of waste biomass. Compared with pyrochar, hydrochar is suitable for dealing with wet biomass directly, with lower energy consumption [19–21]. Hydrochar also has higher yield and cation exchange capacity, and, during the production process, no PAHs are released. On the surface of hydrochar, it has more oxygen-containing functional groups, which is favorable for H₂S capture and oxidation [22,23]. Although hydrochar has such abundant advantages, it has been rarely used to treat gaseous pollutants, especially H₂S.

Chitosan, insoluble in water and organic solvents, is a natural macromolecular aminopolysaccharide with a yield second only to cellulose [24]. Moreover, cornstarch is the world's largest source of starch, accounting for approximately 65% of the total amount worldwide [25]. In this work, chitosan and cornstarch were used to synthesize hydrochar, which was modified by CuO-ZnO in a one-pot process. The aim of this work was to explore the formation of CuO-ZnO on hydrochar, the physical and chemical properties of this new material, the desulfurization products, and the mechanisms. This work provides new insights into the development and application of hydrochar products.

2. Results and Discussion

2.1. Basic Physical and Chemical Properties of Hydrochars

The results of the EDX analyses of the hydrochars are shown in Figure 1. The mass yield (the ratio of product to the original raw biomass), ultimate analysis by EDX (C, O, N, Zn, Cu), specific surface area, pore volume, and average pore diameter are reported in Table 1. It was found that the type of precursor had a significant effect on the yield of hydrochar (Table 1). The mass yields of the solids recovered changed depending on the content and type of the precursor. With the increase in chitosan content, the yield of hydrochar and nitrogen content increased [26], because the hydrochar yield is related to the solubility of the precursors in water, and the solubility of starch is much higher than that of chitosan [24,25]. Simultaneously, the nitrogen in the hydrochar products mainly came from chitosan, and a small amount of nitrogen came from polyacrylamide; therefore, with the increase in the chitosan content, the nitrogen content increased.

Under the same synthetic conditions, when the ratio of chitosan to starch was 1:1, the specific surface area of hydrochar reached 30.102 m²/g. It was found that, although the added amount of ZnCl₂ and CuCl₂ in the precursor was the same, the detected content of Zn in the product was much lower than that of copper. One possible reason is that the pH value of the filtrate during hydrothermal carbonization kept decreasing, and ZnO could not remain stable under the slightly acidic conditions, while CuO was stable under the acidic conditions.

Table 1. The yields, specific surface area, average pore diameter, and elemental composition of the synthesized hydrochars.

Hydrochar	Yield (%)	SSA	PV	APD	Elemental Composition (%)				
					C	O	Zn	Cu	N
S5C5	14.83	30.102	0.071	8.9264	48.49	38.73	0.34	6.68	2.58
S10C0	11.01	12.939	0.041	1.2464	36.42	54.34	0.37	5.57	0.05
S3C7	29.89	16.456	0.069	1.456	38.85	42.07	0.36	6.97	5.93
S7C3	14.44	17.244	0.073	1.6234	43.20	45.37	0.66	5.10	1.18
S0C10	32.37	14.653	0.046	1.093	43.33	39.64	0.41	6.35	7.13
S5C5N	9.7	8.162	0.042	0.891	49.38	36.97	0.42	5.59	2.05

Note: Specific surface area (SSA), Pore volume (PV), Average pore diameter (APD).

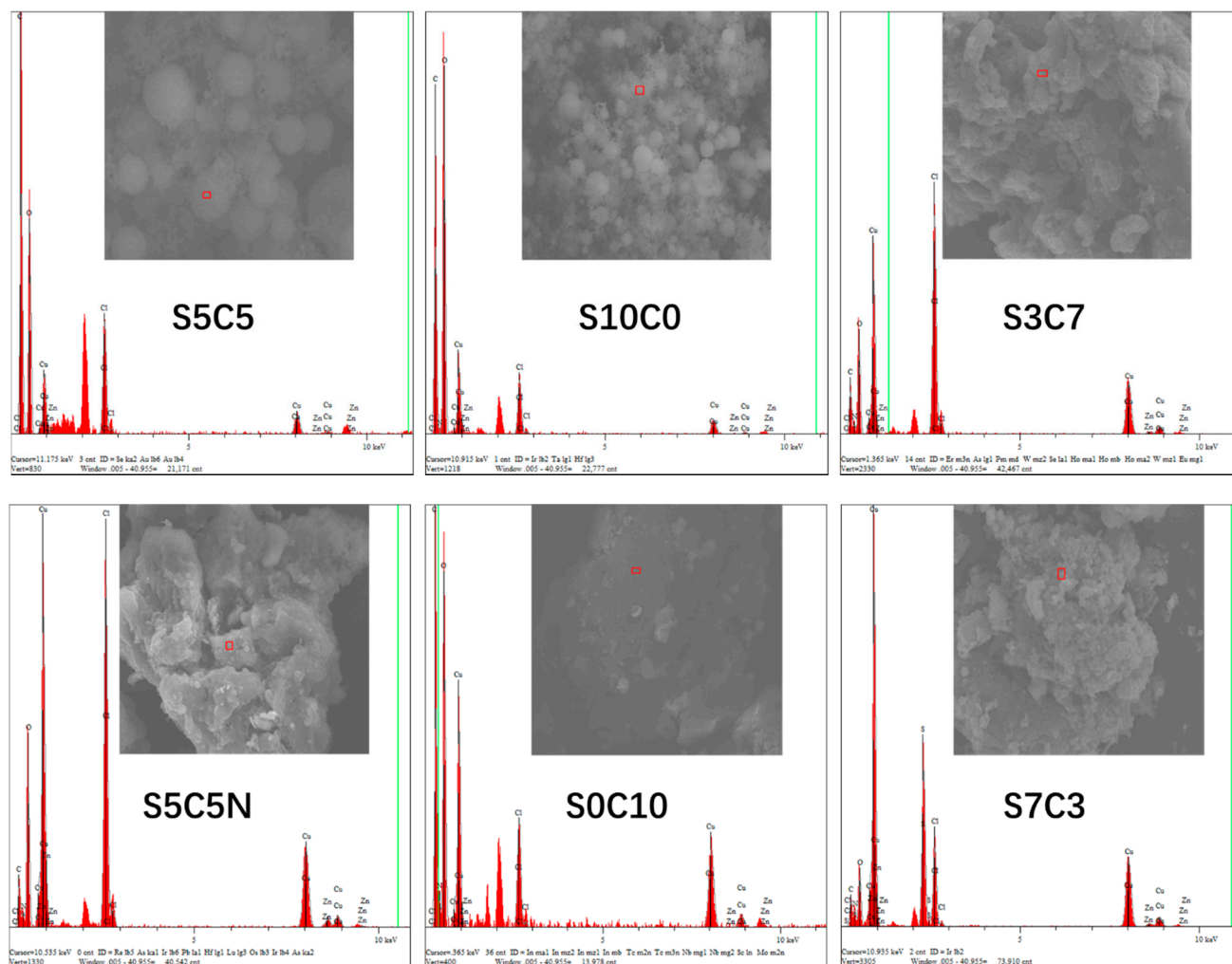


Figure 1. EDX images of the hydrochars.

FT-IR spectra of the hydrochars were used to determine the functional groups contained in the sample, and these are shown in Figure 2. The C=C in aromatic groups showed an adsorption peak between 1613 cm^{-1} and 1718 cm^{-1} . For carbonyl in -COOH and CO-NH, the regions from 1400 cm^{-1} to 1500 cm^{-1} were ascribed to C-N and C-O groups' stretching vibration. The peak at 1033 cm^{-1} was assigned to C-O stretching or O-H bending vibrations. The broad band at 3400 cm^{-1} can be assigned to the existence of the N-H structure. Finally, the peaks at 1033 cm^{-1} and 1403 cm^{-1} were suggested to be C-N and C-O, respectively. According to the elemental analysis and FT-IR analysis, it was proven that amine groups and oxygen-containing groups on the surface of the hydrochar were abundant.

The surface morphology of several hydrochars is shown in Figure 3. It was found that with the change in the starch and chitosan content in the precursors, the hydrochars presented different microstructures. Among all the hydrochars without polyacrylamide, the precursor starch mainly showed carbon particles and carbon spheres with diameters from $10\text{ }\mu\text{m}$ to $100\text{ }\mu\text{m}$, while the precursor chitosan mainly had a porous cellular structure. However, the hydrochar with polyacrylamide was dense, with no regular shape, and consisted of some carbon particles, because both chitosan and cationic polyacrylamide contained positive charges, which could make the distribution of the system more uniform. Furthermore, metal oxide clusters were not observed in any of the photomicrographs. The hydrochar samples with different starch and chitosan content were analyzed by XRD

(in Figure 4), and this showed that the crystallinity of metal oxides in the hydrochar was low. There may be ZnO in S5C5, S5C5N, S10C0, and free Cu in S0C10 due to the reducibility of chitosan [27]. It indicated that the distribution of active metal sites in the hydrochar was relatively uniform or that metal oxides were embedded in carbon spheres or carbon particles [28].

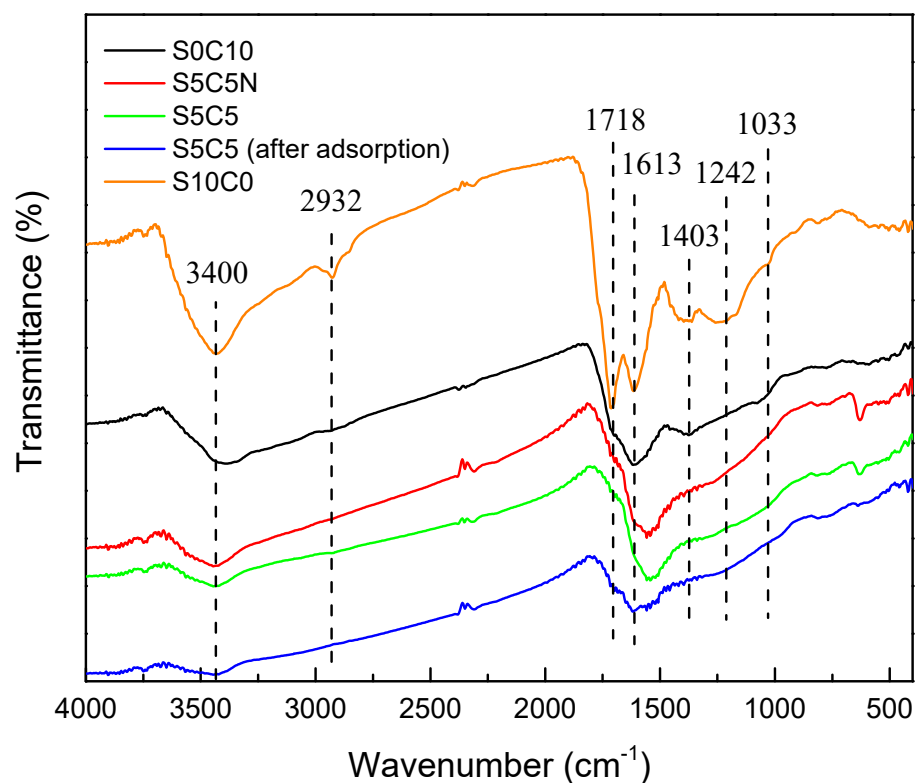


Figure 2. FT-IR spectra of the hydrochars.

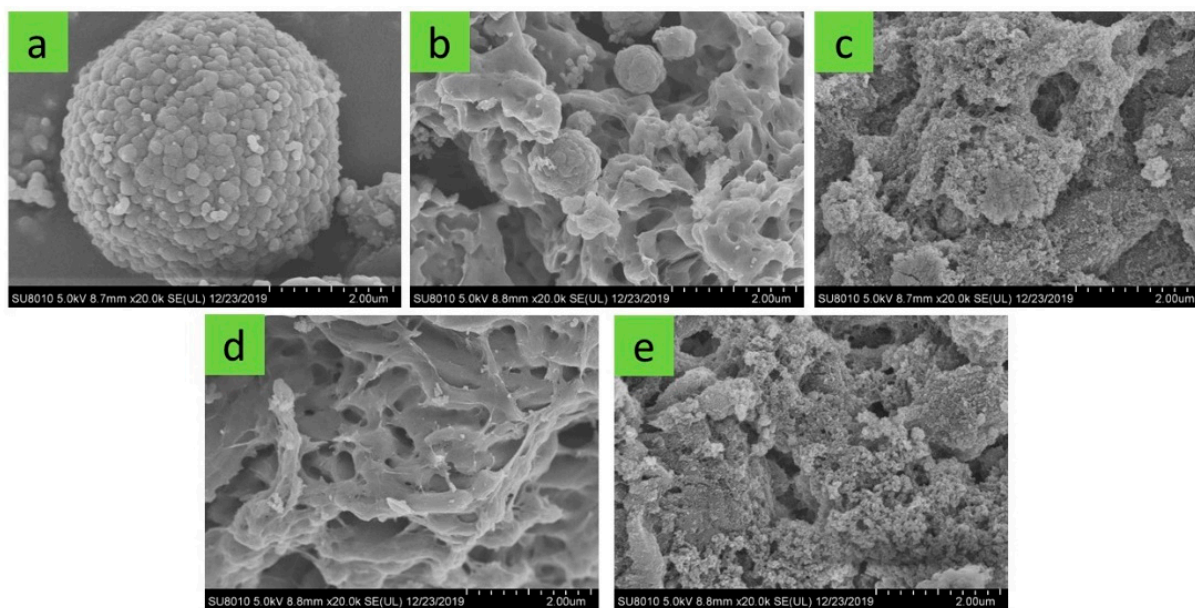


Figure 3. SEM images of different hydrochars. (a) S10C0; (b) S5C5; (c) S5C5N and (d) S0C10 before adsorption; (e) S5C5 after adsorption.

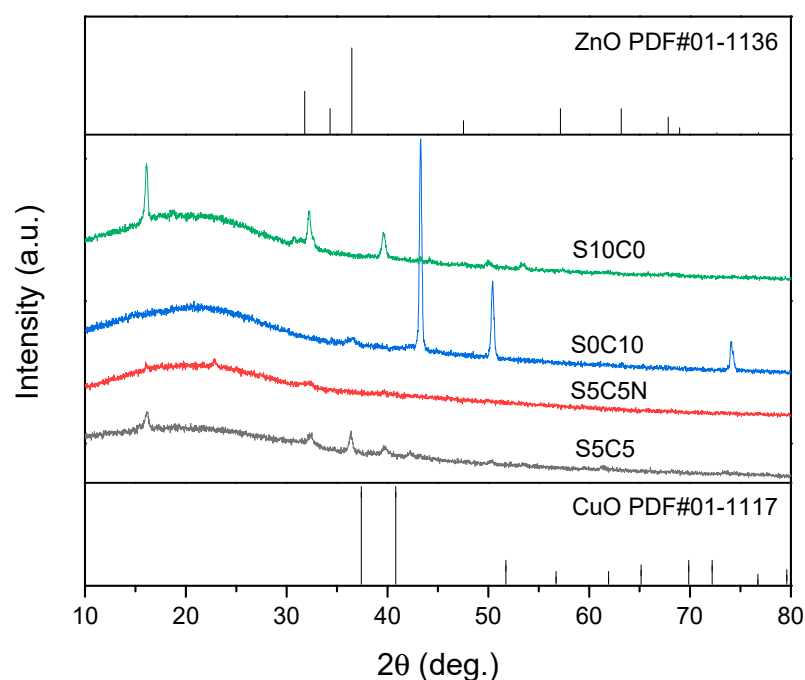


Figure 4. X-Ray diffraction patterns of hydrochar samples.

Notably, no metal oxide aggregates were observed in any of the samples. Based on previous results [29,30], we believe that both the molecular weight and concentration of PAM significantly affected the morphology of the end-products. For the synthesis of nanoporous materials at a large scale, the approach was facile and had many potential applications. In addition, it was also applicable for the synthesis of other materials with a high surface area and nanoporous structures. It has been suggested that the addition of polyacrylamide can affect the morphology of the hydrochar. As an important capping agent, PAM has been widely used to synthesize materials with various nanostructures (nanorods, nanowires, nanoplates, nanocubes, etc.). The exact function of PAM on the shape selectivity is not yet fully understood; however, we believe that the selective adsorption of PAM on various crystallographic planes (newly formed CuO, ZnO, or hydrochar particles) suppressed their intrinsic anisotropic growth [30]. With an N-C=O group, PAM was easily attached to the surfaces of these materials and limited the growth of the crystal faces. Selective interactions between PAM and the different surface planes of the CuO or ZnO may greatly influence the growth direction and rate and ultimately result in particles with different shapes [30]. For an oxidation catalyst, its effectiveness can be mainly attributed to the adsorption and desorption of gas molecules from its surface.

2.2. H_2S Adsorption Performance

2.2.1. Effect of Hydrochar Species

In this section, a series of single-factor experiments were carried out to determine the effect of the adsorbent in the desulfurization system. The H_2S removal efficiency (%) and breakthrough sulfur capacity were selected as the evaluation index. The ratio of chitosan to starch had a significant influence on H_2S removal. The sulfur capacities of hydrochars with different molar ratios of chitosan to starch under 180 °C were measured and are shown in Figure 5. It can be observed that the sulfur capacity of S5C5 was higher than that of other hydrochars and the addition of polyacrylamide had a great impact on H_2S adsorption.

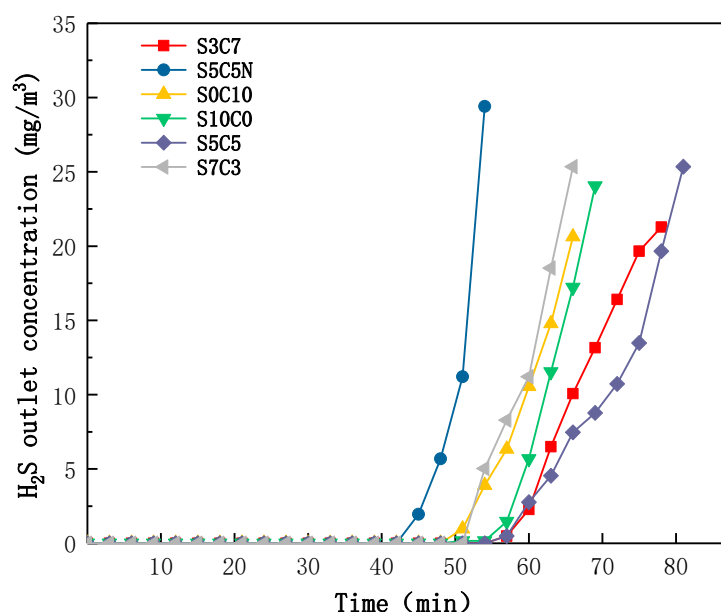


Figure 5. The breakthrough curves of hydrochar S5C5 with different molar ratios of chitosan to starch (T, 230 °C; auxiliary agent, cationic PAM; cationic PAM concentration, 2.0 g/L).

2.2.2. Effect of Auxiliary Agents on H₂S Removal

Cationic PAM, polyvinylpyrrolidone, and neutral PAM were used as the auxiliary agents in the synthesis of the hydrochar. According to the experimental results, it was found that the addition of polyacrylamide and its concentration can affect the sulfur capacity. The effect of different auxiliary agents on H₂S removal by hydrochar S5C5 is shown in Figure 6. Among the three auxiliary agents, the cationic PAM-synthesized hydrochar showed the best performance for H₂S removal. In order to explore the best composition of precursors, the PAM concentrations were also optimized, as shown in Figure 7. With the increasing of the PAM concentration from 0.5 g/L to 3.0 g/L, the sulfur capacity decreased. Cationic PAM with a positive charge can attract to and interact with chitosan of a negative charge, leading to a good combination of cationic PAM in hydrochar, but the best amount of cationic PAM depended on the amount of chitosan.

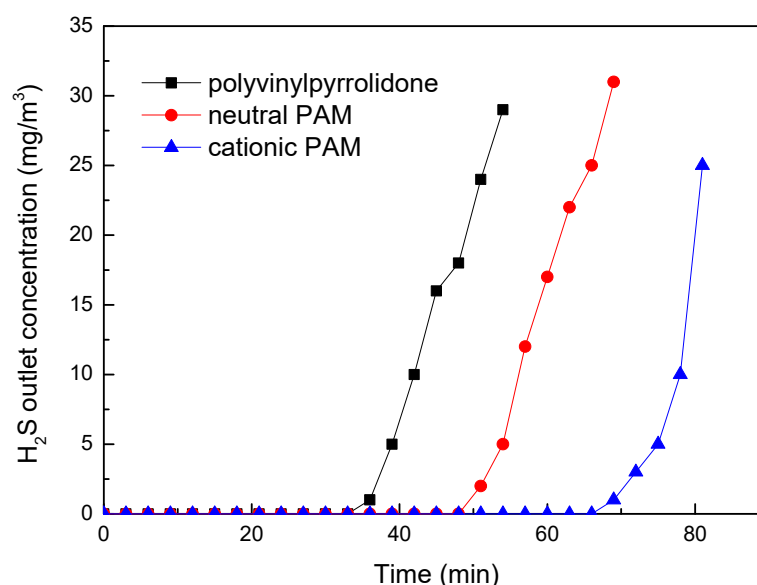


Figure 6. The breakthrough curves of hydrochar S5C5 with different auxiliary agents (T, 230 °C; auxiliary agent concentration, 2.0 g/L).

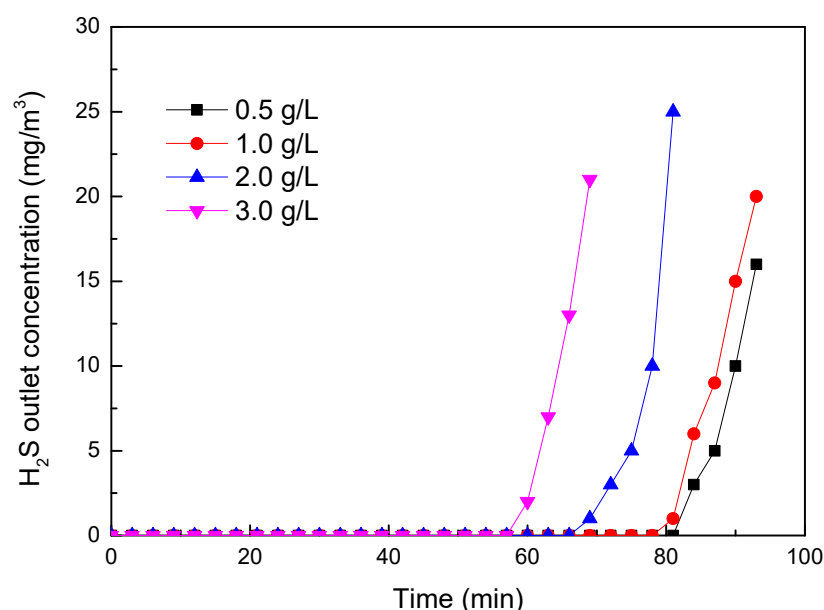


Figure 7. The breakthrough curves of hydrochar S5C5 with cationic PAM of different concentrations (T, 230 °C; auxiliary agent, cationic PAM).

2.2.3. Effect of Adsorption Temperature on H₂S Removal

The effect of adsorption temperature on H₂S removal by hydrochar S5C5 is shown in Figure 8. With the desulfurization temperature increasing, the desulfurization ability of hydrochar S5C5 was clearly improved. This result indicated that the desulfurization ability of S5C5 modified by metal oxide was lower than the sorbent derived from the molecular sieve (SBA-15 or MCM-41) with modification or adsorbents with high metal content; however, it was far higher than other types of common active carbon [31–33]. As is known, a low temperature is beneficial for H₂S adsorption. Raising the temperature could enhance the molecular mobility and interaction between each reactant to promote H₂S adsorption by increasing the reaction rate; however, a higher temperature would be an obstruction to H₂S adsorption in an exothermic reaction.

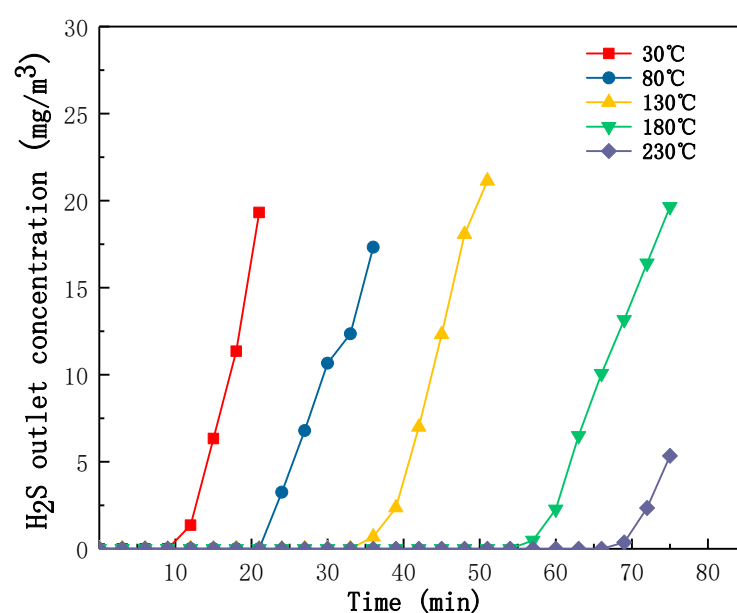


Figure 8. The breakthrough curves of hydrochar S5C5 under different adsorption temperatures (auxiliary agent, cationic PAM; cationic PAM concentration, 0.5 g/L).

In the adsorption and oxidation process of H_2S , the change in the oxygen functional groups on the surface of the hydrochar plays an important role. The quinone and carbonyl groups on the surface of the hydrochar can react with molecular H_2S . The $\text{C}=\text{O}$ bond and $\text{C}=\text{C}$ bond were broken and combined with H_2S to form the $\text{S}-\text{O}$ bond. This process was endothermic and favored the rising temperature. When the ratio of chitosan to starch is 1:1, the cationic PAM concentration is 0.5 g/L, and the temperature is 230°C , the maximum sulfur capacity of the hydrochar S5C5 is 28.06 mg/g-adsorbent.

2.3. Adsorption Mechanism

The adsorption of H_2S on the hydrochar consisted of three parts: the first part is the reaction of H_2S with the metal active sites, such as CuO and ZnO [34]; the second part is the reaction of H_2S with the oxygen-containing functional groups and carbon on the surface of the hydrochar to form $\text{C}-\text{S}$ bonds and $\text{O}-\text{S}$ bonds; the third part is the physical adsorption process of H_2S on the surface of the hydrochar [33].

To further investigate the reaction mechanism, the chemical valence states of the element in the whole process were analyzed by XPS. The XPS spectra of S, Cu, and Zn are shown in Figures 9–11.

The XPS spectrum of S in hydrochar S5C5 after H_2S adsorption is shown in Figure 9. The valence state of S was confirmed within the binding energy in the range of 162–172 eV. This showed that $\text{S } 2p_{3/2}$ and $\text{S}^{2-} 2p_{2/3}$ appeared at 167.5 eV and 161.7 eV, respectively. The peak at 163.4 eV may vary due to the existence of the structure of $\text{C}-\text{S}$ [33]. The Cu^+ was confirmed by the $\text{Cu } 2p_{3/2}$ binding energy in the range of 930 eV to 937 eV, and it showed that $\text{Cu}^+ 2p_{3/2}$ appeared at 932.56 eV, and the Cu^{2+} was assigned to the binding energy of the XPS contribution from 928 to 937 eV with a satellite contribution in the range of 937–947 eV, and it appeared at 934.61 eV. The Zn^{2+} was confirmed by the $\text{Zn } 2p_{3/2}$ that appeared at 1021.77 eV. Therefore, the existing sulfur, zinc, and copper in the hydrochar S5C5 were CuS , ZnS , Cu_2S , sulfur, and a $\text{C}-\text{S}$ bond.

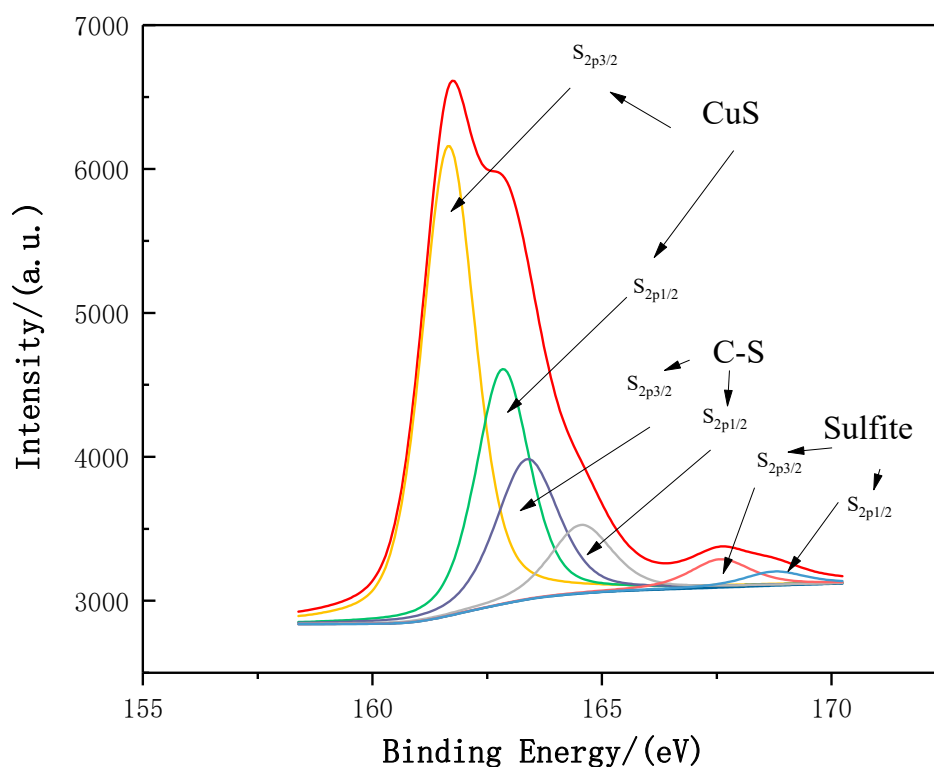


Figure 9. The XPS spectrum of S in hydrochar S5C5 after H_2S adsorption.

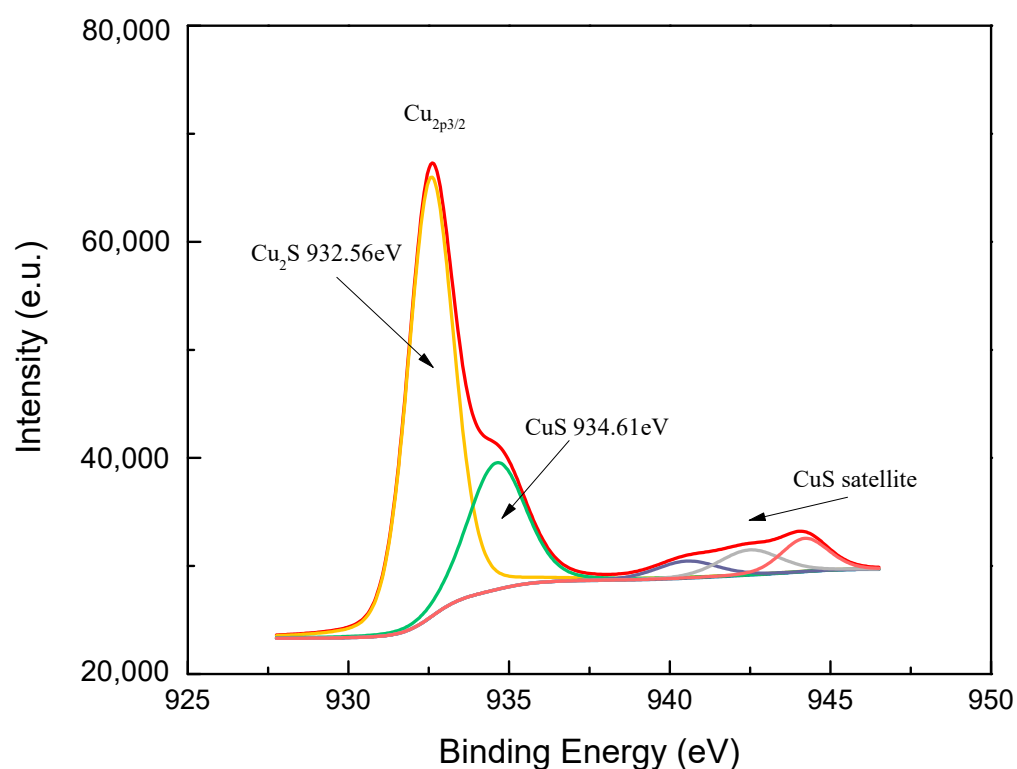


Figure 10. The XPS spectrum of Cu in hydrochar S5C5 after H₂S adsorption.

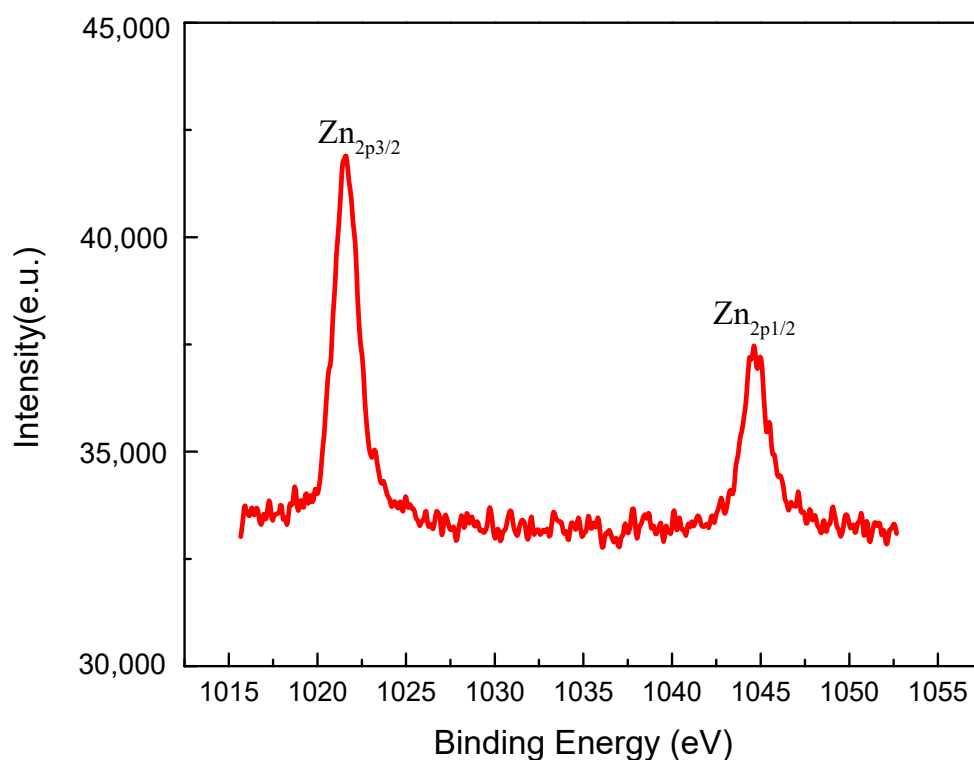


Figure 11. The XPS spectrum of Zn in hydrochar S5C5 after H₂S adsorption.

During the hydrothermal reaction, CuCl₂ and ZnCl₂ reacted to form CuO and ZnO. The reaction equation can be described as follows:



At the same time, copper (II) oxide has a certain oxidation capacity; H_2S can be oxidized partly to elemental sulfur and a fraction of the sulfide ions that have not been oxidized can form Cu_2S [35]. Hydrochar, rich in oxygen-containing functional groups, can combine with H_2S to form a C-S bond and S-O bond [33,36]. Therefore, the form of sulfur after adsorption can be confirmed to be sulfur and a C-S bond. H_2S also can react with oxygen-containing functional groups to form sulfates in the absence of oxygen [33]. There was no oxygen gas to participate in this adsorption, so sulfate did not exist in the product.

3. Materials and Methods

3.1. Materials

The reagents, all of analytical grade, used in this experiment were purchased directly without further purification. Copper chloride, zinc chloride, cationic polyacrylamides (CPAM), and chitosan (low viscosity, deacetylation >90%) were purchased from Shanghai Macklin Biochemical Co., Ltd (Shanghai, China). Cornstarch (Pharmaceutical grade) was purchased from Shanghai Aladdin Biochemical Technology Co., Ltd (Shanghai, China). H_2S standard gas of 1% and N_2 of 99.999% were provided by Jinan Deyang Special Gas Co., Ltd (Jinan, China). The solution was prepared using laboratory-made deionized water ($18.3 \text{ M}\Omega \cdot \text{cm}^{-1}$).

3.2. Preparation of Adsorbent

There were six types of hydrochar synthesized in the experiment. All of them were composed of chitosan and cornstarch, with a cationic polyacrylamide solution (an auxiliary agent) with different dosages. The abbreviation and composition of the synthesized hydrochar samples are shown in Table 2. Taking C5S5 as an example, chitosan (3.60 g), cornstarch (3.60 g), ZnCl_2 (0.84 g), and CuCl_2 (0.84 g) were placed in a mortar, ground evenly with force, and then moved to a glass beaker, following by the addition of 45 mL of cationic polyacrylamide solution (0.5, 1.0, 2.0, and 3.0 g/L). While being treated with ultrasound, the precursors were stirred vigorously until a light blue color appeared. The sample was placed in a hydrothermal reactor and heated up to 230°C for 4 h. The product was washed repeatedly using deionized water until the pH of the rinsed water stabilized. Other hydrochars were synthesized using the same method with different molar ratios of the precursors.

Table 2. Abbreviations and compositions of six kinds of hydrochar.

Sample	Carbon Precursor (Dosage)	Auxiliary Agent	Metal Oxide Precursor (Dosage)
S5C5	Starch (3.60 g) + Chitosan (3.60 g)	Cationic polyacrylamide solution	ZnCl_2 (0.84 g) + CuCl_2 (0.84 g)
S10C0	Starch (7.20 g)		
S3C7	Starch (2.16 g) + Chitosan (5.04 g)		
S7C3	Starch (5.04 g) + Chitosan (2.16 g)		
S0C10	Chitosan (7.20 g)		
S5C5N	Starch (3.60 g) + Chitosan (3.60 g)	None	

3.3. Characterization of Hydrochar

The characterization of materials was investigated using a Fourier-transform infrared (FTIR) spectrophotometer (IRAffinity-1s, Shimadzu, Kyoto, Japan). X-ray diffraction (XRD) patterns of hydrochar samples were recorded on an X-ray diffractometer (SmartLab, Rigaku, Tokyo, Japan) and carried out in the 2θ range from 10° to 80° . The surface morphologies of materials were observed by scanning electron microscope (SEM) apparatus (Regulus 8220, Hitachi, Tokyo, Japan). The element composition and valence state of materials were explored by X-ray photoelectron spectroscopy (XPS) with a multifunctional imaging electron spectrometer (ESCALAB 250XI, Thermo Fisher, Waltham, MA, America). The specific surface areas of materials were measured using the Brunauer–Emmett–Teller (BET) method, and the pore size distribution was calculated using the Barrett–Joyner–Halenda (BJH) method from the isotherm of the adsorption branch with an automatic specific surface area and porosity analyzer (TriStar II 3020, Micromeritics, Norcross, GA, USA).

3.4. Batch H_2S Adsorption Experiments

The mixed gas was prepared by blending H_2S standard gas with N_2 , both quantified by flow indicators (D08-1F), which were purchased from Beijing Sevenstar Electronics Co., Ltd. (Beijing, China); the concentration of H_2S was measured by the gas analyzer (TH-990S) from Wuhan Tianhong Instrument Group. After adsorption, the sulfur capability was calculated by Equation (1):

$$H_2S \text{ removal efficiency}(\%) = \frac{C_{in} - C_{out}}{C_{in}} \times 100\% \quad (5)$$

C_{in} and C_{out} ($\text{mg} \cdot \text{m}^{-3}$) were the inlet and outlet concentration of H_2S in the gas mixture, respectively. A diagram of the test devices for the evaluation of desulfurization performance is shown in Figure 12.

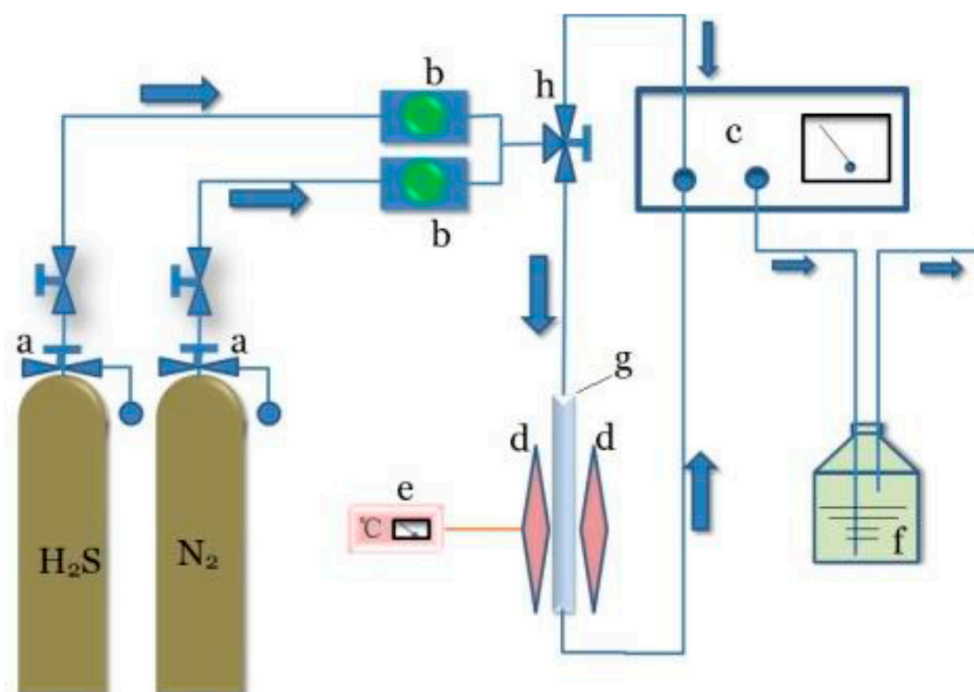


Figure 12. The diagram of test devices for the evaluation of desulfurization performance. (a) Pressure reducing valve; (b) mass flow controller; (c) portable hydrogen sulfide concentration analyzer; (d) tube furnace; (e) temperature controller; (f) concentrated lye; (g) quartz tube; (h) three-way valve.

To test sulfur capacity, a quartz tube was used and its diameter and height were 6 mm and 100 mm, respectively. The adsorption temperature was controlled by a tube furnace. In the tests, a gas mixture containing 3000 ppm (4617 mg/m^3) of H_2S (nitrogen as balance

gas) was passed through the quartz tube filled with adsorbent of 0.5 g, under a gas flow rate of 100 mL/min. The outlet H₂S gas was absorbed by KOH solution. The breakthrough sulfur capacity (S_b , mg/g) was calculated in the stage from the beginning to when the H₂S outlet concentration was higher than 20 mg/m³ by Equation (2).

$$S_b = \frac{M_S}{M_{H_2S}} \times \frac{Q_{H_2S}}{m} \left[\int_0^t (C_{in} - C_{out}) dt \right] \times 10^{-6} \quad (6)$$

where S_b represents the breakthrough sulfur capacity of sorbents (mg/g), M_S and M_{H_2S} are the molar weight of sulfur (32.06 g/mol) and H₂S (34.06 g/mol), respectively; m is the weight of sorbents; Q_{H_2S} is the H₂S gas flow rate; t is the reaction time for desulfurization (min), and C_{in} and C_{out} are the inlet and outlet concentration of H₂S (mg/m³), respectively. When t is the saturation adsorption time, Equation (2) was also used to calculate the max sulfur capacity (C_m).

4. Conclusions

For H₂S adsorption, this study provides a method for the synthesis of hydrochar, obtained by the hydrothermal reaction of chitosan, starch, cationic polyacrylamide aqueous solution, ZnCl₂, and CuCl₂. The experimental results showed that the hydrochar contained many amino groups as functional groups, and the nano-scaled metal oxide particles had good dispersion on the surface of the hydrochar. The amine group significantly reduced the activation energy of H₂S and CuO-ZnO, which was conducive to the rapid diffusion of H₂S among the lattices. At the same time, cationic polyacrylamide as a steric stabilizer can change the formation process of CuO and ZnO nanoparticles, making the particle size smaller and allowing it to react more easily with H₂S sufficiently. When the ratio of chitosan to starch is 1:1, the temperature is 230 °C, and the cationic PAM concentration is 0.5 g/L, the maximum sulfur capacity of the hydrochar S5C5 is 28.06 mg/g-adsorbent. Therefore, modified hydrochar may be a promising adsorbent for H₂S removal.

Author Contributions: Conceptualization, Y.M. and L.Z.; methodology, J.M. and C.Z.; software, R.X.; validation, Y.M. and L.Z.; formal analysis, L.W.; resources, L.D. and L.Z.; data curation, J.M. and Y.M.; writing—original draft preparation, J.M., C.Z. and Y.M.; writing—review and editing, X.L.; funding acquisition, L.D. and L.Z. All authors have read and agreed to the published version of the manuscript.

Funding: This work was funded by the Open Research Fund Program of Key Laboratory of Cleaner Production and Integrated Resource Utilization of China National Light Industry, grant number CP-2020-YB8, Natural Science Foundation of Shandong Province, grant number ZR2020QB199, and Qilu University of Technology (Shandong Academy of Sciences) Youth Doctor Cooperation Fund, grant number 2019BSHZ0028.

Conflicts of Interest: The authors declare no conflict of interest.

References

- Coenen, K.; Gallucci, F.; Hensen, E.; Annaland, M.V.S. Adsorption behavior and kinetics of H₂S on a potassium-promoted hydrotalcite. *Int. J. Hydrog. Energy* **2018**, *43*, 20758–20771. [\[CrossRef\]](#)
- Garcia-Arriaga, V.; Alvarez-Ramirez, J.; Amaya, M.; Sosa, E. H₂S and O₂ influence on the corrosion of carbon steel immersed in a solution containing 3M diethanolamine. *Corros. Eng.* **2010**, *52*, 2268–2279. [\[CrossRef\]](#)
- Xiao, Y.H.; Wang, S.D.; Wu, D.Y.; Yuan, Q. Experimental and simulation study of hydrogen sulfide adsorption on impregnated activated carbon under anaerobic conditions. *J. Hazard. Mater.* **2008**, *153*, 1193–1200. [\[CrossRef\]](#) [\[PubMed\]](#)
- Eow, J.S. Recovery of sulfur from sour acid gas: A review of the technology. *Environ. Prog. Sustain. Energy* **2010**, *21*, 143–162. [\[CrossRef\]](#)
- Zhao, T.; Yao, Y.; Li, D.; Wu, F.; Zhang, C.; Gao, B. Facile low-temperature one-step synthesis of pomelo peel biochar under air atmosphere and its adsorption behaviors for Ag(I) and Pb(II). *Sci. Total Environ.* **2018**, *640–641*, 73–79. [\[CrossRef\]](#)
- Zhang, X.; Dou, G.Y.; Wang, Z.; Li, L.; Wang, Y.F.; Wang, H.L.; Hao, Z.P. Selective catalytic oxidation of H₂S over iron oxide supported on alumina-intercalated Laponite clay catalysts. *J. Hazard. Mater.* **2013**, *260*, 104–111. [\[CrossRef\]](#) [\[PubMed\]](#)
- Yasyerli, S. Cerium–manganese mixed oxides for high temperature H₂S removal and activity comparisons with V–Mn, Zn–Mn, Fe–Mn sorbents. *Chem. Eng. Process. Process Intensif.* **2008**, *47*, 577–584. [\[CrossRef\]](#)

8. Khudenko, B.M.; Gitman, G.M.; Wechsler, T.E.P. Oxygen Based Claus Process for Recovery of Sulfur from H₂S Gases. *J. Environ. Eng.* **1993**, *119*, 1233–1251. [[CrossRef](#)]
9. Garces, H.F.; Galindo, H.M.; Garces, L.J.; Hunt, J.; Morey, A.; Suib, S.L. Low temperature H₂S dry-desulfurization with zinc oxide. *Microporous Mesoporous Mater.* **2010**, *127*, 190–197. [[CrossRef](#)]
10. Zhang, X.; Tang, Y.Y.; Qu, S.Q.; Da, J.W.; Hao, Z.P. H₂S-Selective Catalytic Oxidation: Catalysts and Processes. *ACS Catal.* **2015**, *5*, 1053–1067. [[CrossRef](#)]
11. Liu, Z.; Wang, Z.; Chen, H.; Cai, T.; Liu, Z. Hydrochar and pyrochar for sorption of pollutants in wastewater and exhaust gas: A critical review. *Environ. Pollut.* **2021**, *268*, 115910. [[CrossRef](#)]
12. Bridgwater, A.V.; Meier, D.; Radlein, D. An Overview of Fast Pyrolysis of Biomass. *Org. Geochem.* **1999**, *30*, 1479–1493. [[CrossRef](#)]
13. Liang, J.; Shan, G.C.; Sun, Y.F. Catalytic fast pyrolysis of lignocellulosic biomass: Critical role of zeolite catalysts. *Renew. Sustain. Energy Rev.* **2021**, *139*, 110707. [[CrossRef](#)]
14. Hardy, B.; Leifeld, J.; Knicker, H.; Dufey, J.E.; Deforce, K.; Cornélis, J.-T. Long term change in chemical properties of preindustrial charcoal particles aged in forest and agricultural temperate soil. *Org. Geochem.* **2017**, *107*, 33–45. [[CrossRef](#)]
15. Luz, F.C.; Volpe, M.; Fiori, L.; Manni, A.; Cordiner, S.; Mulone, V.; Rocco, V. Spent coffee enhanced biomethane potential via an integrated hydrothermal carbonizationanaerobic digestion process. *Bioresour. Technol.* **2018**, *256*, 102–109.
16. Liu, Y.X.; Yao, S.; Wang, Y.Y.; Lu, H.H.; Brar, S.K.; Yang, S.M. Bio- and hydrochars from rice straw and pig manure: Inter-comparison. *Bioresour. Technol.* **2017**, *235*, 332–337. [[CrossRef](#)]
17. Xiao, X.; Chen, B.L.; Chen, Z.M.; Zhu, L.Z.; Schnoor, J.L. Insight into Multiple and Multi-level Structures of Biochars and Their Potential Environmental Applications: A Critical Review. *Environ. Eng. Technol.* **2018**, *52*, 5027–5047.
18. Sun, P.Z.; Li, Y.X.; Meng, T.; Zhang, R.C.; Song, M.; Ren, J. Removal of sulfonamide antibiotics and human metabolite by biochar and biochar/H₂O₂ in synthetic urine. *Water Res.* **2018**, *147*, 91–100. [[CrossRef](#)] [[PubMed](#)]
19. Liu, Z.G.; Balasubramanian, R. Upgrading of waste biomass by hydrothermal carbonization (HTC) and low temperature pyrolysis (LTP): A comparative evaluation. *Appl. Energy* **2014**, *114*, 857–864. [[CrossRef](#)]
20. Titirici, M.M.; White, R.J.; Falco, C.; Sevilla, M. Black perspectives for a green future: Hydrothermal carbons for environment protection and energy storage. *Energy Environ. Sci.* **2012**, *5*, 6796. [[CrossRef](#)]
21. Brunner, G. Near critical and supercritical water. Part I. Hydrolytic and hydrothermal processes. *J. Supercrit. Fluids* **2009**, *47*, 373–381. [[CrossRef](#)]
22. Xia, Y.; Yang, T.X.; Zhu, N.M.; Li, D.; Chen, Z.L.; Lang, Q.Q.; Liu, Z.G.; Jiao, W.T. Enhanced adsorption of Pb(II) onto modified hydrochar: Modeling and mechanism analysis. *Bioresour. Technol.* **2019**, *288*, 121593. [[CrossRef](#)]
23. Dawood, S.; Sen, T.K.; Phan, C. Synthesis and characterization of slow pyrolysis pine cone bio-char in the removal of organic and inorganic pollutants from aqueous solution by adsorption: Kinetic, equilibrium, mechanism and thermodynamic. *Bioresour. Technol.* **2017**, *246*, 76–81. [[CrossRef](#)] [[PubMed](#)]
24. Simsir, H.; Eltugral, N.; Karagoz, S. Hydrothermal carbonization for the preparation of hydrochars from glucose, cellulose, chitin, chitosan and wood chips via low-temperature and their characterization. *Bioresour. Technol.* **2017**, *246*, 82–87. [[CrossRef](#)] [[PubMed](#)]
25. Wang, B.; Gao, W.; Kang, X.M.; Dong, Y.Q.; Liu, P.F.; Yan, S.X.; Yu, B.; Guo, L.; Cui, B.; El-Aty, A.M.A. Structural changes in corn starch granules treated at different temperatures. *Food Hydrocoll.* **2021**, *118*, 106760. [[CrossRef](#)]
26. Tekin, K.; Karagöz, S.; Bektaş, S. A review of hydrothermal biomass processing. *Renew. Sustain. Energy Rev.* **2014**, *40*, 673–687. [[CrossRef](#)]
27. Almughamisi, M.S.; Khan, Z.A.; Alshitari, W.; Elwakeel, K.Z. Recovery of chromium(VI) oxyanions from aqueous solution using Cu(OH)₂ and CuO embedded chitosan adsorbents. *J. Polym. Environ.* **2020**, *28*, 47–60. [[CrossRef](#)]
28. Xu, X.W.; Huang, G.Q.; Qi, S. Properties of AC and 13X zeolite modified with CuCl₂ and Cu(NO₃)₂ in phosphine removal and the adsorptive mechanisms. *Chem. Eng. J.* **2017**, *316*, 563–572. [[CrossRef](#)]
29. Peng, Y.; Liu, Z.Y.; Yang, Z.H. Polymer-Controlled Growth of CuO Nanodiscs in the Mild Aqueous Solution. *Chin. J. Chem.* **2009**, *27*, 1086–1092. [[CrossRef](#)]
30. Zhou, M.; Gao, Y.; Wang, B.; Rozynek, Z.; Fossum, J.O. Carbonate-Assisted Hydrothermal Synthesis of Nanoporous CuO Microstructures and Their Application in Catalysis. *Eur. J. Inorg. Chem.* **2010**, *5*, 729–734. [[CrossRef](#)]
31. Mureddu, M.; Ferino, I.; Rombi, E.; Cutrufello, M.G.; Deiana, P.; Ardu, A.; Musinu, A.; Piccaluga, G.; Cannas, C. ZnO/SBA-15 composites for mid-temperature removal of H₂S: Synthesis, performance and regeneration studies. *Fuel* **2012**, *102*, 691–700. [[CrossRef](#)]
32. Dhage, P.; Samokhvalov, A.; Repala, D.; Duin, E.C.; Bowman, M.; Tatarchuk, B.J. Copper-Promoted ZnO/SiO₂ Regenerable Sorbents for the Room Temperature Removal of H₂S from Reformate Gas Streams. *Ind. Eng. Chem. Res.* **2010**, *49*, 8388–8396. [[CrossRef](#)]
33. Li, Y.R.; Lin, Y.T.; Xu, Z.C.; Wang, B.; Zhu, T.Y. Oxidation mechanisms of H₂S by oxygen and oxygen-containing functional groups on activated carbon. *Fuel Process. Technol.* **2019**, *189*, 110–119. [[CrossRef](#)]

-
34. Falco, D.G.; Montagnaro, F.; Balsamo, M.; Erto, A.; Deorsola, F.A.; Lisi, L.; Cimino, S. Synergic effect of Zn and Cu oxides dispersed on activated carbon during reactive adsorption of H₂S at room temperature. *Microporous Mesoporous Mater.* **2018**, *257*, 135–146. [[CrossRef](#)]
 35. Kim, S.-J.; Na, C.W.; Hwang, I.-S.; Lee, J.-H. One-pot hydrothermal synthesis of CuO–ZnO composite hollow spheres for selective H₂S detection. *Sens. Actuators B Chem.* **2012**, *168*, 83–89. [[CrossRef](#)]
 36. Boutillara, Y.; Tombeur, J.L.; De Weireld, G.; Lodewyckx, P. In-situ copper impregnation by chemical activation with CuCl₂ and its application to SO₂ and H₂S capture by activated carbons. *Chem. Eng. J.* **2019**, *372*, 631–637. [[CrossRef](#)]